Journal of Controlled Release 253 (2017) 172–182

Contents lists available at ScienceDirect

Journal of Controlled Release

journal homepage: www.elsevier.com/locate/jconrel

Optical barcoding of PLGA for multispectral analysis of nanoparticle fate *in vivo*

David X. Medina [a], Kyle T. Householder [a,b], Ricki Ceton [a,b], Tina Kovalik [a], John M. Heffernan [a,b], Rohini V. Shankar [b], Robert P. Bowser [a], Robert J. Wechsler-Reya [c], Rachael W. Sirianni [a,b,*]

[a] Barrow Brain Tumor Research Center, Barrow Neurological Institute, 350 W Thomas Road, Phoenix, AZ 85013, USA
[b] School of Biological and Health Systems Engineering, Arizona State University, P.O. Box 879709, Tempe, AZ 85287, USA
[c] Sanford Burnham Prebys Medical Discovery Institute, 2880 Torrey Pines Scenic Drive, La Jolla, CA 92037, USA

ARTICLE INFO

Article history:
Received 14 July 2016
Received in revised form 8 February 2017
Accepted 27 February 2017
Available online 3 March 2017

Keywords:
Quantum-dots
PLGA nanoparticles
Imaging and tracking
Multispectral
Cell-penetrating peptide
Targeting

ABSTRACT

Understanding of the mechanisms by which systemically administered nanoparticles achieve delivery across biological barriers remains incomplete, due in part to the challenge of tracking nanoparticle fate in the body. Here, we develop a new approach for "barcoding" nanoparticles composed of poly(lactic-co-glycolic acid) (PLGA) with bright, spectrally defined quantum dots (QDs) to enable direct, fluorescent detection of nanoparticle fate with subcellular resolution. We show that QD labeling does not affect major biophysical properties of nanoparticles or their interaction with cells and tissues. Live cell imaging enabled simultaneous visualization of the interaction of control and targeted nanoparticles with bEnd.3 cells in a flow chamber, providing direct evidence that surface modification of nanoparticles with the cell-penetrating peptide TAT increases their biophysical association with cell surfaces over very short time periods under convective current. We next developed this technique for quantitative biodistribution analysis *in vivo*. These studies demonstrate that nanoparticle surface modification with the cell penetrating peptide TAT facilitates brain-specific delivery that is restricted to brain vasculature. Although nanoparticle entry into the healthy brain parenchyma is minimal, with no evidence for movement of nanoparticles across the blood-brain barrier (BBB), we observed that nanoparticles are able to enter to the central nervous system (CNS) through regions of altered BBB permeability – for example, into circumventricular organs in the brain or leaky vasculature of late-stage intracranial tumors. In sum, these data demonstrate a new, multispectral approach for barcoding PLGA, which enables simultaneous, quantitative analysis of the fate of multiple nanoparticle formulations *in vivo*.

1. Introduction

It has been observed that drug encapsulation within solid nanoparticles can improve therapy in a variety of disease models [1,2], although how these improvements are achieved, particularly in privileged sites such as the brain, remains under active debate. The mechanisms by which nanoparticles improve the action of systemically administered compounds include solubilization of hydrophobic agents to enable delivery of drugs at doses that could not otherwise be safely administered; protection of encapsulated molecules from clearance, inactivation, and degradation *via* sustained release; or enablement of drug delivery across highly restrictive biological barriers, such as the blood brain barrier (BBB) or blood tumor barrier (BTB) [4–8]. Surface modification of nanoparticles to facilitate tissue-specific delivery is a popular strategy for enhancing efficacy of systemically administered therapies; this approach has been utilized successfully in a range of preclinical models, as measured by improved pharmacokinetic profiles or biological activity of specific drugs [6,9]. However, conventional approaches to study drug delivery from targeted nanoparticles can lead to incomplete conclusions or misinterpretation of delivery of the nanoparticle *versus* the distribution and activity of a specific payload [10–13]. For example, we recently demonstrated that the use of small molecules for biodistribution analysis can be highly misleading: loading two different molecules into the same surface-modified nanoparticle led to opposite conclusions regarding the kinetics of brain-specific delivery [11]. These data confirm prior *in vitro* reports demonstrating that encapsulated small molecules leach rapidly from solid nanoparticles into cellular membranes [13]. Thus, biodistribution analysis of non-covalently linked agents will be specific to each agent, which makes the development of a generalizable platform for drug delivery difficult. Covalent labeling of polymers with

* Corresponding author at: Neuroscience Research Center, NRC 436, 350 W Thomas Rd, Phoenix, AZ 85013, USA.
E-mail address: rachael.sirianni@dignityhealth.org (R.W. Sirianni).

http://dx.doi.org/10.1016/j.jconrel.2017.02.033

small molecule fluorophores or radioligands is one alternative. However, conventional fluorophores suffer from poor sensitivity, photobleaching, and signal loss during tissue processing, which makes detection in low-concentration sites (such as the brain) difficult Autoradiography, while attractive for its superb sensitivity, requires specialized experimental approaches that are not easy to broadly implement [14].

It is perhaps unsurprising that extensive debate remains regarding the ability of nanoparticles (*versus* encapsulated payload) to cross biological barriers such as the BBB [11,15]. A growing body of evidence suggests that new methods will be required to understand the distinct fate of nanoparticle *versus* encapsulated payload in the body [11,13,16]. Here, our goal was to develop a sensitive, multiplex approach for direct evaluation of the fate of polymeric nanoparticles *in vivo*, which we predict will improve our ability to understand the interaction of surface-modified nanoparticles with biological barriers such as the BBB and BTB. We hypothesize that "barcoding" polymeric nanoparticles with spectrally defined quantum dots will enable simultaneous analysis of multiple nanoparticle formulations in individual cells or organisms. Quantum dots (QDs) have been used extensively to label peptides, antibodies and other macromolecules, and their tightly defined emission spectrum facilitates multiplex detection [17,18]. In addition, optical barcoding strategies have already been employed by many others to enable multiplex biosensing and tissue staining [19–21]. Thus, we chose to link parent poly(lactic-co-glycolic acid) (PLGA) to commercially available, amine-functionalized/poly(ethylene glycol (PEG) coated quantum dots of varying emission wavelength. QD-PLGA was blended with PLGA to form a library of quantum dot-labeled nanoparticles such that each nanoparticle possesses distinct emission wavelength to enable multiplex detection. Our data demonstrate that biophysical properties of the quantum dot labeled nanoparticles (herein QD-NPs) were not changed by attachment of quantum dots, and we show application of the method for both qualitative and quantitative localization of multiple nanoparticle formulations in individual samples with very high spatial resolution and detection sensitivity. We propose that the ability to track nanoparticles at the cellular level is an important tool that, in parallel with traditional tracking methods, can be used to form a more comprehensive understanding of both drug delivery and nanoparticle fate *in vivo*.

2. Methods and materials

2.1. Materials

TAT-biotin peptide (sequence: Biotin-YGRKKRRQRRR) was synthesized by GenScript (Piscataway, CA, USA). 50:50 Poly(DL-lactide-co-glycolide) (PLGA, ester terminated, 0.55–0.75 IV) and 50:50 Poly(DL-lactide-co-glycolide) (PLGA, carboxyl-terminated, 0.55–0.75) were obtained from Lactel Absorable Polymers (Birmingham, AL, USA). Amino (PEG) Quantum dots were purchased from Thermo Fisher Scientific (Waltham, MA, USA). Polyvinyl alcohol (PVA; MW = 30 kDa–70 kDa; 87–90% hydrolyzed) was purchased from Sigma-Aldrich (St. Louis, MO, USA). All other reagents for nanoparticle preparation were purchased from Sigma-Aldrich (St. Louis, MO, USA). Cell culture reagents (DMEM, FBS) were purchased from Life Technologies (Carlsbad, CA, USA).

2.2. PLGA conjugation to QDs

15 mg of carboxylic acid terminated PLGA (375 nmoles) were dissolved in 1.5 mL dimethylformamide (DMF). 1-Ethyl-3-(3-dimethylaminopropyl) carbomiidide (EDC) (6.2 mg), N-Hydroxysuccinimide NHS (4.5 mg) and 120 μL of 8 μM QDs (0.96 nmoles) were added to dissolved PLGA in DMF and stirred for 24 h at room temperature. This yielded a ratio of 375 nmol of PLGA-COOH to 0.96 nmol QD. After 24 h, the mixture was added dropwise to 50 mL DI water and centrifuged for 30 min, 5000 RCF at 4 °C; we confirmed that these centrifugation conditions were sufficient to wash free (non-conjugated) QDs from the polymer. The supernatant was removed, and the resulting pellet was collected and lyophilized overnight. The lyophilized PLGA-QD was stored at −20 until it was used to formulate nanoparticles. ^{1}H NMR spectroscopy (400 MHz Varian Inova, Aglient Technologies, Santa Clara, CA, USA) was used to confirm synthesis of PLGA-QD polymers. NMR samples were prepared at a concentration of 10 mg/mL in $CDCl_3$.

2.3. Nanoparticle fabrication

Nanoparticles were produced by single emulsion-solvent evaporation with slight modification [22]. Briefly, 90 mg ester-terminated PLGA and 10 mg PLGA-QD was dissolved in 1 mL of dichloromethane (DCM). The dissolved PLGA was added dropwise into 2 mL of 5% (w/v) PVA under vortexing and probe sonicated (Fisher Scientific Model 705 Sonic Dismembrator, Waltham, MA, USA) on ice in 3, 10-s bursts at 40% amplitude. The resulting emulsion was added to 50 mL of 0.3% PVA and stirred for 3 h to evaporate solvent. Nanoparticles were collected by centrifugation for 25 min at 25,000 RCF and the resulting nanoparticle pellet was washed three times with DI water. The final nanoparticle pellet was resuspended in 3 mL DI water containing 25 mg trehalose, frozen and lyophilized overnight. To produce QD-NPs loaded with Nile red (NR), 90 mg ester-terminated PLGA, 10 mg PLGA-QD, and 2.5 mg of NR were dissolved in 1 mL of DCM. The dissolved PLGA and NR were added dropwise into 2 mL of 5% (w/v) PVA under vortexing and probe sonicated as described above.

2.4. Surface modification of QD-NPs

PLGA nanoparticles were prepared by single emulsion method as described above, blending PLGA-QD with parent ester terminated PLGA and incorporating avidin-palmitate in the primary emulsion to enable surface modification. Avidin-palmitate conjugation was performed as previously described [11]. Briefly, 25 mg of avidin was reacted to palmitic acid-NHS overnight while stirring at 37 °C in 2% w/v sodium deoxycholate in PBS. Avidin-palmitic acid conjugate was purified by 48 h dialysis against 0.15% w/v sodium deoxycholate in PBS (MW cutoff of 14 kDa). To generate avidin containing QD-NPs, 90 mg of ester-terminated PLGA and 10 mg PLGA-QD was dissolved in 1 mL of DCM. This solution was added drop-wise into 2 mL of 5% (w/v) PVA containing 5 mg/mL avidin-palmitate under vortexing and sonicated on ice in 3, 10-s bursts at 40% amplitude. The resulting emulsion was added to 50 mL of 0.3% PVA and stirred for 3 h to evaporate solvent. Nanoparticles were collected by centrifugation for 20 min at 25,000 RCF and the resulting nanoparticle pellet was washed and centrifuged 2×. For surface modification, nanoparticles were incubated with a 10× molar excess of Biotin-TAT (QD-NP-TAT) or biotin (QD-NP-Biotin) for 1 h. This approach is expected to generate nanoparticles with up to several hundred biotin-binding sites for peptide linkage [11,23]. Nanoparticles were washed by centrifugation to remove excess ligand. A small sample was removed for TEM characterization and trehalose (25 mg per 100 mg PLGA) was added to the remaining nanoparticle solution as a cryoprotectant. The nanoparticle solution was aliquoted, frozen, lyophilized and stored at −80 °C.

2.5. Nanoparticle characterization

Hydrodynamic diameters and zeta-potentials of QD-NPs were determined using dynamic light scattering (DLS) using a NanoBrook 90 Plus Zeta(Brookhaven) and BIC Particle Solutions software. Lyophilized nanoparticles were resuspended in 1 mM KCL to a concentration of 1 mg/mL. Nanoparticle solutions were placed in a sonication bath for 15 min. Transmission Electron Microscopy (TEM) was performed to determine distribution of QDs within PLGA nanoparticles. A JEOL 1200 microscope was used at an accelerating voltage of 80 kV and

a magnification of 120 k. Specimens were prepared by dipping a mesh copper grid into a 0.1 mg/mL suspension of nanoparticles. The grid was then dried prior to imaging. The number of QDs per nanoparticle was manually counted from TEM images for 130 individual nanoparticles.

2.6. Stability assay

Nanoparticles labeled with QDs emitting at 585 nm (herein referred to as NP_{585}) and loaded with Nile Red were resuspended at a concentration of 0.5 mg/mL by sonication bath for 15 min in 50% fetal bovine serum. Nanoparticles where then incubated in 500 μL aliquots in 1.5 mL microcentrifuge tubes at 37 °C for 15 min, 30 min, 2 h, 4 h or 24 h after resuspension. After incubation, tubes were centrifuged at 5000 *g* for 10 min. The supernatant was collected and the pellet was resuspended. 50 μL of each sample were plated in triplicate and measured with a plate reader. Fluorescence of Nile Red and NP_{585} were measured separately (552/636 nm and 305/585 nm excitation/emission, respectively). The signals from the supernatant and pellet were combined, and percentage of total signal were calculated for each.

2.7. Cell viability assay

HEK293 cells were plated in a 96 well flat clear bottom white polystyrene TC-treated plate at a density of 3000 cells per well in phenol free DMEM + 5% FBS. The cells were allowed to adhere overnight. Unlabeled nanoparticles or QD-NPs were reconstituted in the same media. Cells were treated in triplicate for 16 h with nanoparticle concentrations from 0.1 mg/mL to 16 mg/mL. Viability was determined by Promega CellTiter-Glo Luminescent Cell Viability assay. Cells and assay buffers were equilibrated to room temp and treated accordingly. Luminescence was read on a Tecan Infinite 2000 plate spectrophotometer.

2.8. Cell uptake

HEK293 cells were seeded at a density of 500 k cells/well in 6-well plates and allowed to attach overnight in DMEM + 10% FBS. Normal media was then replaced with 1.5 mL of DMEM + 1% FBS containing 1 mg/mL nanoparticles. Cells were incubated with QD-NP containing media for 2,6 or 24 h in triplicate. Following incubation, media was aspirated from cells. Cells were washed with PBS and trypsinized, then collected with DMEM + 10% FBS. Cells were spun down at 100 RCF for 5 min, and the supernatant was removed. Cells were resuspended in PBS and pelleted 2 more times. After washing, cells were lysed by incubation in RIPA buffer at 37 °C for 1 h. The cell lysate was pelleted by centrifugation at 25,000 RCF for 30 min at 4 °C. The pellet was resuspended in 200 uL PBS. Fluorescence of 50 μL of the pellet suspension were read, in triplicate, on black flat bottom 96 well plate using a Tecan Infinite 2000 plate spectrophotometer (Ex/Em 305/585 and 305/655 for NP_{585} and NP_{655}, respectively). The concentration of nanoparticles was determined by normalizing fluorescence to cell number collected from each well and comparing it to a control curve constructed by spiking non-treated cell extract with known amounts of QD-NPs.

2.9. In vivo QD-NP administration

Nanoparticle tissue distribution was examined *in vivo* in BalbC mice (Charles River, Wilmington, MA). All procedures and animal care practices were performed in accordance with the Barrow Neurological Institute's Institutional Animal Care and Use Committee. For the confocal microscopy experiments, 2-month-old mice (n = 5) were injected *via* lateral tail vein with 4 mg of QD-NP or 8 mgs of a QD-NP mixture of (4 mg each of QD-NP_{585} and NP_{655}) and sacrificed 2 h post injection. Mice were anesthetized and perfused with cold PBS and tissues were collected and placed in 4% PFA for 48 h. Tissue was cryoprotected by immersing tissue in 30% sucrose for 48 h at 4 °C. Tissue sections were made at a thickness of 16 μm using a cryostat and mounted on charged microscope slides. Immunofluorescence was performed on sections using CD31 (Abcam, Cambridge, MA, USA) to determine QD-NPs localization in relation to endothelial cells. Sections were coverslipped using Vectashield with DAPI. Sections were imaged with using an Observer Z1 confocal microscope (Zeiss) and Zen 2009 software. The 405 excitation laser was used to visualize QD-NPs. For biodistribution analysis, 2-month-old mice (n = 7) were injected *via* lateral tail vein with 4 mg of QD-NP or 8 mg of a QD-NP mixture of (4 mg each of QD-NP_{585} and NP_{655}) and sacrificed 2 h post injection. Blood samples were collected *via* cardiac puncture, and mice were perfused with cold PBS. Liver, spleen, and whole brain were immediately collected following perfusion and stored at −80 °C until further processing. Tissue was thawed on ice and finely minced with a razor blade into a pulp. DiH20 was added to the pulp to make a final concentration of 10% w/v. Tissue was physically disrupted in a bead homogenizer for 10 min at the highest speed and lysed by probe sonication (10 s pulses, 2×) on ice. Tissue homogenates (50 μL) were added to a 96-well plate with 10 μL of dimethyl sulfoxide (DMSO). Fluorescence intensity was read on a Tecan Infinite 2000 plate spectrophotometer (Ex/Ex 305/585 and 305/655 for NP_{585} and NP_{655}, respectively). Quantification of QD-NP delivery was determined by converting AU values to concentration by generating control curves for each organ by spiking control tissue homogenates with known quantities of QD-NPs.

2.10. Live cell imaging

Laminar μ-Slide I Luer 0.4 ibiTreat flow chambers (Ibidi, Germany) were used for laminar flow experiments. At least 24 h before experiments bEnd.3 cells were seeded in the chambers and allowed to grow to 80–90% confluency. On the day of the experiment TAT-NP_{655} and CTL-NP_{585} were resuspended to a concentration of 0.125 mg/mL (0.0625 mg/ml of each nanoparticle formulation in 40 mL of media) in 1% FBS Fluorobrite© DMEM. Cells were stained with the live cell marker calcein-am to help with locating and focusing microscope to cell surface. Live cell imaging was performed using an Observer Z1 confocal microscope (Zeiss) and Zen 2009 software. Media with nanoparticles was flowed into the chambers at 0.25 mL/min, 1 mL/min or 4 mL/min for 15 min. Recordings began immediately prior to the start of media infusion.

2.11. Tumor induction

Tumor inductions were performed as previously described [3,24]. Albino C57BL/6 mice (Envigo, Indianapolis, IN, USA) were anesthetized with an intraperitoneal injection of ketamine (100 mg/kg) and xylazine (10 mg/kg) and mounted on a small animal stereotaxic instrument (Model 900, Kopf Instruments, Tujunga, CA, USA). Animal temperature was maintained using a circulating water heating pad placed beneath the frame. A sterile surgical field was obtained by three alternating passes of betadine solution and 70% isopropanol over the surgical site. An incision was made down the midline of the scalp to expose the skull, and a burr hole was drilled to target the striatum (2 mm lateral and 0.1 mm posterior from bregma). A Hamilton syringe filled with 2 μL of the cell suspension (75 k GL261 cells) was lowered to a depth of 3 mm and allowed to equilibrate with tissue for 1 min. The syringe was then withdrawn to a depth of 2.6 mm and the cells were infused at a rate of 1 μL/min. The syringe was left in place for 1 min before it was removed to reduce back flow. The incision was closed using staples and a triple antibiotic ointment was applied to the scalp before placing the animal in a clean cage over a heating pad to recover. All animals received a single subcutaneous (SQ) injection of buprenorphine (0.1 mg/kg) immediately after surgery and ibuprofen was provided in their drinking water for 1 week post-op to control pain.

3. Results and discussion

3.1. Generation and characterization of quantum dot-labeled nanoparticles

QDs were conjugated to PLGA-COOH *via* EDC/NHS chemistry (Fig. 1A). This conjugation chemistry has been described by others [25], however, when we followed this published protocol, nanoparticles were not sufficiently bright to enable reliable *in vivo* imaging. We therefore increased the QD:PLGA ratio by a factor of 10 to yield a more brightly labeled polymer. ^{1}H NMR analysis confirmed the conjugation of QD to the carboxyl end of PLGA (Fig. S1). To generate labeled nanoparticles, QD-PLGA was blended with ester-terminated PLGA in a 1:9 ratio prior to nanoparticle formation by single emulsion [22,25]. Empirical measurement of pre- and post-fabrication fluorescence yielded labeling of 3.87×10^{-11} mol QD per 100 mg of nanoparticle, which equates to an encapsulation efficiency of ~40%. Transmission electron microscopy (TEM) confirmed that nanoparticles formed as expected, with QDs distributed throughout the nanoparticle (Fig. 1B and Fig. S2). Nearly all nanoparticles observed under TEM were labeled with at least one QD, with the average nanoparticle containing 12.5 (±1.9) QDs. This labeling allowed for robust visualization of QD-NPs using fluorescent microscopy.

QD emission wavelength is directly related to QD diameter, which ranges from 2 to 20 nm [26]; for the wavelength of QDs utilized in this work, the manufacturer-reported diameter is 16–19 nm. To test whether QD attachment or type altered biophysical properties of the nanoparticle generated from QD-labeled polymer, we measured hydrodynamic diameter and zeta potential of QD-nanoparticles suspended in 1 mM KCl. Non-modified nanoparticles possessed an average diameter of 255 nm and average zeta potential of 3.9 mV; neither presence nor type of QD significantly affected the size or zeta potential of labeled nanoparticles above typical batch to batch variability (Table 1). These data demonstrate QD labeling performed under these conditions does not significantly affect the major biophysical characteristics of the nanoparticles.

Table 1
Characterization of QD-NPs.

Nanoparticle formulation	Size (nm)	PDI	Zeta potential (mV)
Blank NP	255 (±3.1)	0.13	3.9
NP_{525}	266 (±1.5)	0.13	−3.8
NP_{545}	272 (±2.3)	0.11	−6.91
NP_{585}	254 (±1.8)	0.10	−3.88
NP_{605}	235 (±2.6)	0.09	−2.88
NP_{655}	252 (±2.8)	0.12	−4.07
NP_{705}	282 (±4.4)	0.17	−6.44
NP_{800}	278 (±3.2)	0.14	−6.75
TAT-NP_{585}	280 (±2.4)	0.12	−2.97
CTL-NP_{655}	296 (±1.6)	0.12	−4.65

To test whether polymer conjugation affected the fluorescent properties of QDs, we analyzed the emission spectrum of QD-NPs labeled with QD_{585}, QD_{605}, QD_{655} and QD_{705} (herein referred to as NP_{585}, NP_{605}, NP_{655} and NP_{705}) (Fig. 1C & Fig. S3). We observed a small blue shift in peak emission for NP_{605} compared to free QD_{605} (Fig. S3). These data confirm a similar observation previously reported by Pederzoli, et al. [27]. However, shifts in peak emission were not observed in NP_{585}, NP_{655} or NP_{705}. The anomalous blue shift for QD_{605} was reproducible across experimental replicates and present for intact nanoparticles and DMSO dissolved nanoparticles. Pederzoli, et al. observed a similar spectral shift and attributed it to particle fabrication; however, our data would suggest that the shift is both unique to QD_{605} and directly related to its conjugation to PLGA, rather than being a function of the particle fabrication. We confirmed in other experiments that spectral properties of QD-labeled nanoparticles were unchanged by attachment of the targeting ligand, TAT (data not shown).

3.2. Nanoparticle fate in cells and tissues

In early work, we attempted to load freely-suspended, non-PEGylated QDs into PLGA nanoparticles; these formulations induced cell death within hours of incubation, achieving complete cell kill even

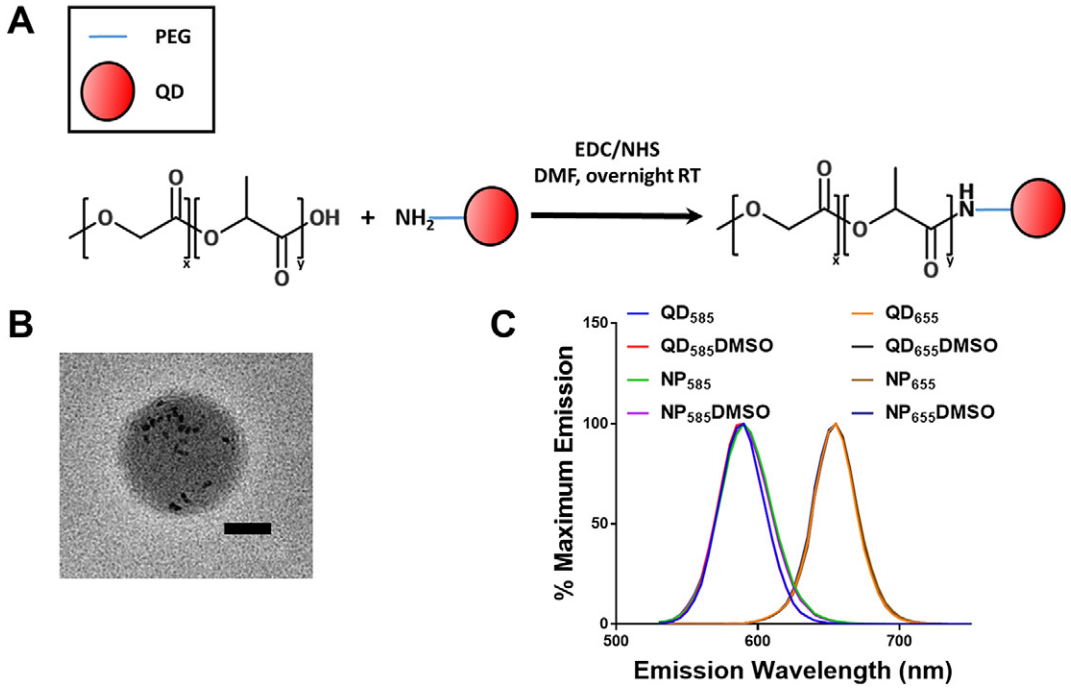

Fig. 1. Fabrication and characterization of covalently linked QD-PLGA nanoparticles. (A) Schematic demonstrating the processes of labeling PLGA-COOH with QD-PEG-amino. Nanoparticles were formed *via* single emulsion/solvent evaporation method by mixing QD labeled polymer 1:9 ratio with ester-terminated PLGA. (B) Transmission electron microscopy image of quantum dot labeled nanoparticles (scale bar represents 50 nm). (C) Emission scans of free QD (585 or 655) or QD linked to PLGA in nanoparticles (NP_{585} or NP_{655}). Scans reveal no large shifts in the emission spectra of free QD *vs* linked QD. Excitation wavelength was set at 405 nm.

at relatively low nanoparticle concentrations (*e.g.*, 1 mg/mL, data not shown). It is likely that the non-covalently linked QDs were readily released from the surface of the nanoparticle to produce this toxicity. Although bare QDs possess well-known toxicity, which has been attributed to cadmium release and oxidative stress, surface modification with poly(ethylene glycol) (PEG, PEGylation) is an accepted method to reduce this toxicity [28]; further, we reasoned that conjugation to PLGA would provide additional protection against toxicity by increasing the relative incorporation/retention of QDs within the protected nanoparticle core. TEM data suggest that a portion of the QDs could be exposed on the surface of the nanoparticle (Fig. 1B). We therefore expected that QD toxicity would be present if QD-NPs were applied at a high enough concentration but predicted that it would be possible to utilize QD-nanoparticles under conditions where cell viability would not be affected. To identify the threshold for QD-NP induced toxicity, we incubated HEK cells with increasing concentrations of NP_{655} and measured viability after 24 h (Fig. 2A). QD-NPs caused significant reduction in viability at the rather high concentration of ≥8 mg/mL after 24 h compared to non-treated cells. This toxicity was not seen in cells treated with control nanoparticles that had no QDs (Fig. S4A), and the toxicity threshold was similar for differently barcoded nanoparticles (data not shown). Based on these results, all subsequent experiments were conducted on cells incubated with no >1 mg/mL QD-NPs, which is both a typical concentration for uptake experiments and far below the concentration at which we have observed cytotoxicity.

Transfer of nanoparticle-encapsulated payload can occur over a time scale of minutes, whereas actual internalization of nanoparticles is believed to take place over hours [13]. Thus, a major goal of this study was to test whether QD labeling would enable independent tracking of nanoparticle *versus* encapsulated payload fate within cells. To accomplish this goal, we generated QD-labeled nanoparticles that also encapsulated Nile red (NR), a hydrophobic dye commonly used for the purpose of tracking nanoparticle delivery. HEK cells, selected for their common use in drug delivery work, were incubated with NR loaded QD-NPs at a concentration of 1 mg/mL at 37 °C and imaged after different time points after exposure (Fig. 2B). Widespread cytoplasmic staining was observed in the NR channel after 15 min of incubation, which was the earliest time point tested.

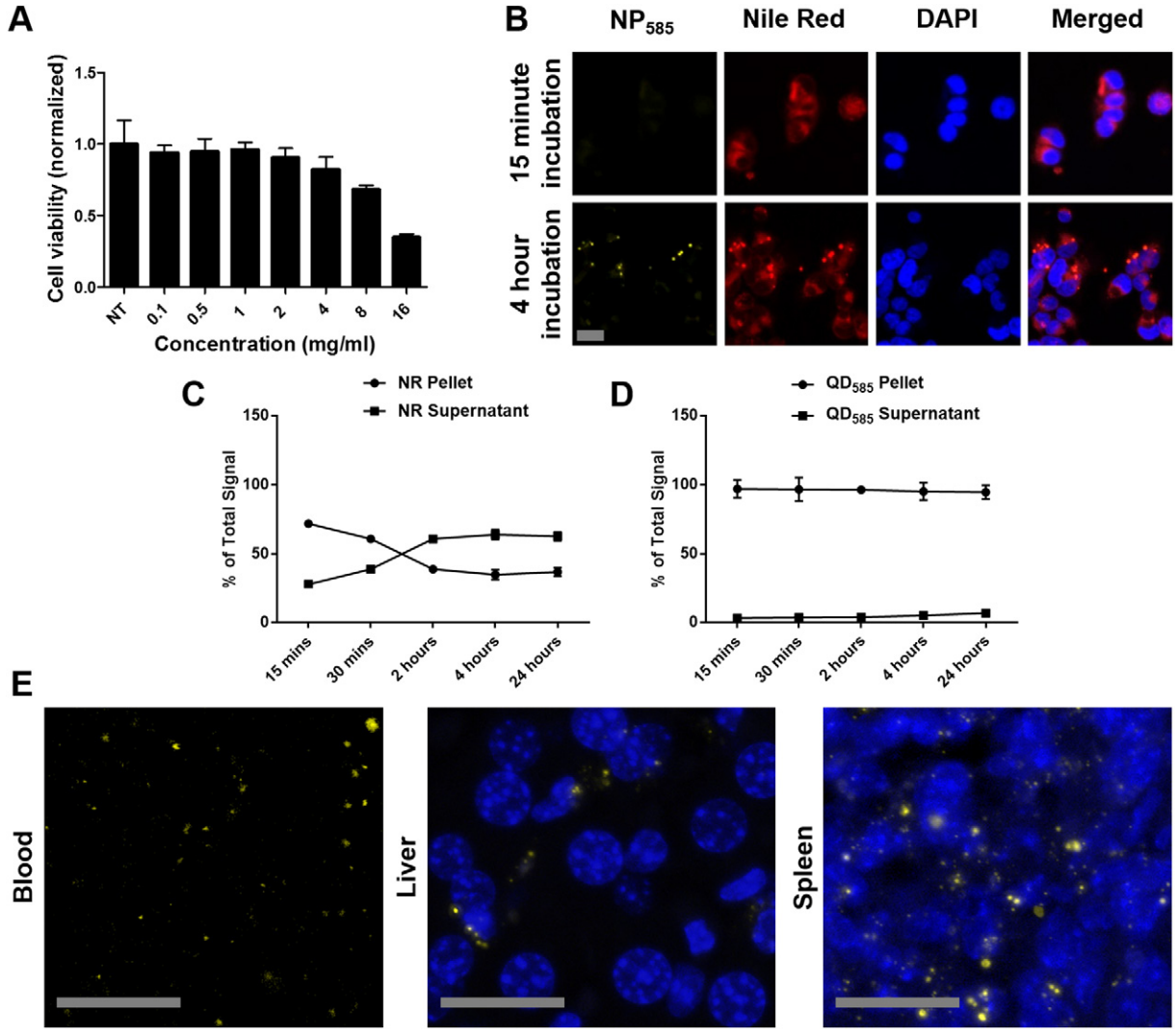

Fig. 2. QD-labeled nanoparticles fates *in vitro* and *in vivo*. (A) Cell viability assay showed that QD-NPs demonstrated significant toxicity compared to non-treated cells starting at a cell media concentration of 8 mg/mL after 24 h. Error bars show standard deviation of the mean. (B) Nile Red (NR) loaded NP_{585} were incubated with HEK cells at a concentration of 1 mg/mL. NR rapidly leaches into cells after 15 min. However, signal from NP_{585} is not found in cells until after 4 h, thus demonstrating that the internalization of the QD-labeled nanoparticle is far less rapid than NR. (C–D) Stability assay to determine stability of NR and QD_{585} within NPs. Fluorescence was measured after incubation at different time points in 50% serum at 37 °C. NR is quickly releases into supernatant, while the QD signal is maintained within the pellet over 24 h. (E) *In vivo* distribution of NP_{585} in the blood, liver and spleen 2 h post systemic administration demonstrates the robust signal that can be obtained in different tissues using confocal microscopy. Scale bars = 20 μm.

We observed similarly non-specific leaching for nanoparticles that were loaded with coumarin 6 (Fig. S4B), demonstrating that the rapid leaching was not unique to NR. Thus, even when encapsulated molecules are not released in aqueous environments, they are capable of leaching rapidly into membranes once the nanoparticles are exposed to cells [10,11,13]. In contrast, signal in the QD_{585} channel was only observed after several hours; the QD signal was characterized as individually distinct puncta within the cytoplasm with no diffuse signal. Analysis of z-stacks confirmed that the QD signal was intracellular. Every QD punctum was co-localized with a NR punctum, although some NR puncta did not overlap with QD signal. This colocalization of NR and QD signal could indicate that some NR that remains encapsulated within QD-NPs, although we cannot exclude the possibility that organelles containing QD-NPs are stained non-specifically by NR that has already been released or leached directly from the particle. To test whether the punctate QD signal could be due to QDs not linked to the nanoparticle, we incubated cells with freely suspended QDs. Uptake of freely suspended QDs was not observed after 2 h of incubation; after 24 h of incubation, signal was characteristically dim, diffuse throughout the cytoplasm, and not punctate (Fig. S4C). Taken collectively, these data demonstrate that QD-nanoparticle internalization can be detected with subcellular resolution *in vitro* and also emphasize the distinct fate of nanoparticle *versus* encapsulated payload in cells. To further confirm stability of the QD-NP linkage under physiological conditions, nanoparticles that were either loaded with NR or linked to QDs were re-suspended in 50% serum and incubated at 37 °C. We first identified centrifugation conditions under which freely suspended QDs were not pelleted. Next, at various time points, samples were subjected to centrifugation to separate the nanoparticle pellet and supernatant. Approximately 30% of the NR was detected in the supernatant after 15 min, and this value increased over time (Fig. 2C–D). In contrast, the QD_{585} signal remained in the pellet, with almost no fluorescence detectable in the supernatant, even after 24 h. This experiment provides further confirmation that QDs remained stably linked under physiological conditions.

We next tested whether this approach would yield sufficient detection sensitivity to track QD-NPs *in vivo*. When we followed previously published protocols, we found that QD-labeled nanoparticles were not bright enough to be readily detected *in vivo* [25]; however, the formulations discussed here were produced by increasing the concentration of QDs during initial the conjugation step of PLGA-COOH to QDs, which enabled sensitive detection of QD-NPs in tissue. To evaluate tissue level delivery, QD-NPs were administered at a standard dose (200 mg/kg) to healthy Balb/c mice *via* lateral tail vein injection. After 2 h, mice were euthanized and saline perfused to clear blood. Liver, spleen, brain and spinal cord were fixed and processed for *ex vivo* confocal analysis. Microscopic analysis revealed that QDs were readily detectable in blood smears, liver and spleen as expected (Fig. 2E), although QD-NPs could not be reliably identified in most regions of the parenchyma of the brain or spinal cord.

3.3. Multispectral analysis of QD-NP fate in cells and tissue

One advantage of using QDs for labeling is that they could enable simultaneous tracking of more than one nanoparticle formulation at a time with minimal signal overlap between channels. To determine whether internalization of multiple nanoparticle formulations could be distinguished by individual color, we incubated HEK cells with 1:1 ratios of nanoparticles bearing distinct QD spectra (NP_{655} or NP_{800}). Punctate signals were observed independently in the expected wavelengths with no spectral bleed-through of fluorescence from one channel to another. Interestingly, QD puncta were rarely, if ever, colocalized; these data suggest that punctate signals reflect individual endocytotic events (either single nanoparticles or single aggregates of nanoparticles) (Fig. 3A). To evaluate uptake quantitatively, cells were simultaneously exposed to a mixture of NP_{585}, NP_{655}, and NP_{800}, washed, lysed and read at the appropriate wavelength on a fluorescent plate reader. Fluorescent signal increased by an equivalent fraction between 2 and 6 h for cells incubated with NP_{585} (0.65, ±0.15), NP_{655} (0.98, ±0.39) and those incubated with NP_{800} (0.85, ±0.26) (Fig. 3B). Thus, we observed

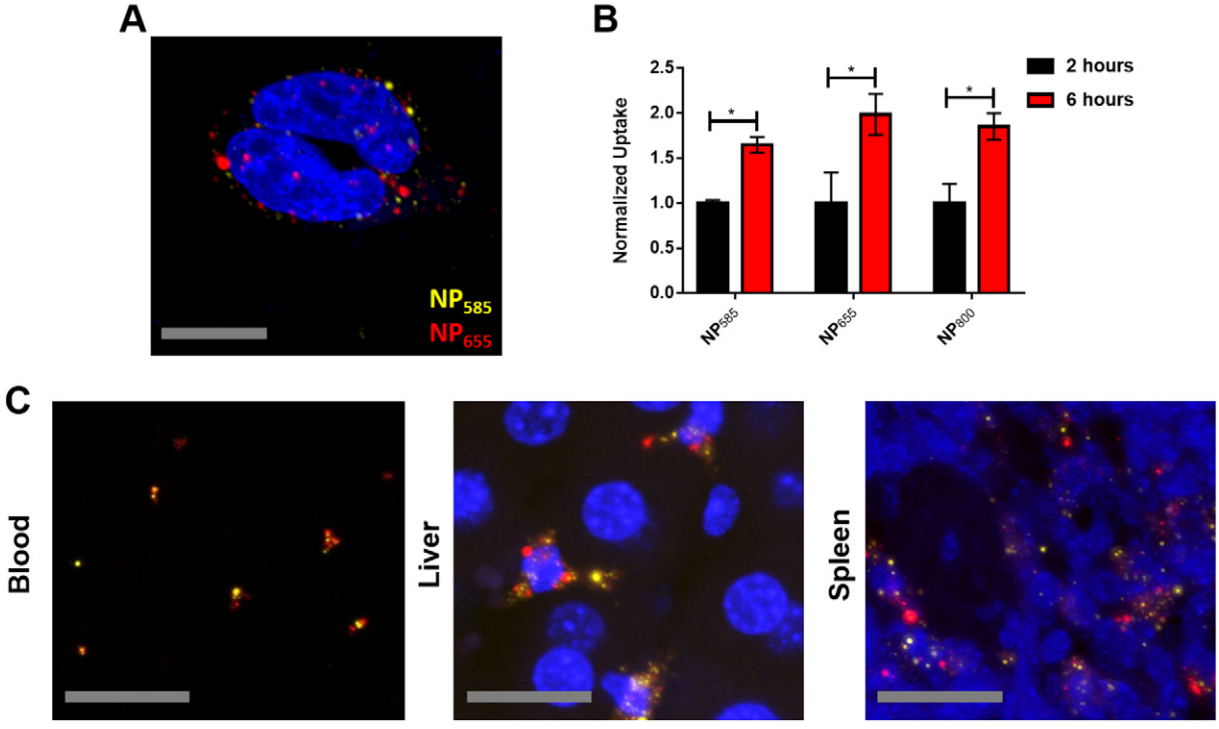

Fig. 3. QD-NPs used to track multiple formulations of nanoparticles in single subjects *in vitro* and *in vivo*. (A) Intracellular NP_{585} and NP_{655} signals are observed with similar qualitative abundance in HEK293 cells after a 6-h incubation. (B) Fluorescent readings of cell lysates show similar increases in fluorescence from after 2 to 6 h incubations with either NP_{585}, NP_{655} or NP_{800}. Error bars show standard deviation of the mean. (C) Multiple QD-NPs (NP_{585} and NP_{655}) were detected simultaneously in different tissue samples, including blood, liver, and spleen, demonstrating the ability to optically track multiple formulations *in vivo* using confocal microscopy. Scale bar = 20 μm.

no evidence that the type of QD attached to the nanoparticle significantly affects its interaction with cells. Given that the QDs are PEGylated and at least partially shielded within the nanoparticle, this result is expected; presumably the dominating factor in nanoparticle uptake will be the biophysical property of the nanoparticle itself.

We next tested whether multispectral microscopy could be used to localize multiple nanoparticle formulations *in vivo*. NP_{655} and NP_{585} were administered simultaneously *via* lateral tail vein injection to healthy mice and tissues were examined 2 h later. Similar to our prior experiments injecting a single type of QD-NP, nanoparticles were readily detected in the liver, spleen and blood after 2 h. There were no qualitative differences in cellular level distribution of differently colored formulations (Fig. 3C). To determine whether QD-NPs could be extracted from tissue for quantitative analysis, we administered a 1:1 mixture of NP_{655} and NP_{585} to healthy mice, which were then saline perfused to enable fluorescent readout of organ homogenates. While optimizing the biodistribution procedures, we determined that the fluorescence intensity of the nanoparticles was reduced in a QD-specific manner during our extraction protocols (data not shown). To account for signal differences resulting from the extraction protocols, we constructed all control curves from pre-spiked tissues samples that were then subjected to the same buffers, tissue homogenization and centrifugations steps as experimental samples. Under these conditions, quantitative extraction confirmed equivalent concentration of differently labeled nanoparticles in organs of interest (Fig. 4A–C), with results expressed as mg nanoparticle per g tissue. The highest amounts of QD-NPs were found in the spleen with NP_{655} and NP_{585} being found at 4.33 ± 0.48 mg/g and 5.09 ± 0.75 mg/g. Levels of QD-NPs in the liver were 0.75 ± 0.11 mg/g tissue and 0.86 ± 0.15 mg/g for NP_{655} and NP_{585}, respectively. Levels of QD-NPs were the lowest in the brain, with 0.026 ± 0.0028 mg/g and 0.031 ± 0.003 mg/g for NP_{655} and NP_{585} respectively. We performed a traditional biodistribution analysis, averaging across experimental groups (Fig. 4A–C); these data demonstrated that there was no significant difference in nanoparticle concentration in various organs when measured by NP_{585} or NP_{655} ($p = 0.36$, 0.43, and 0.25 for liver, spleen, and brain, respectively, unpaired 2-tailed Student's *t*-test; *p* values remained insignificant when analyses were performed on paired data; Fig. S5). Altogether, we find no evidence that the presence

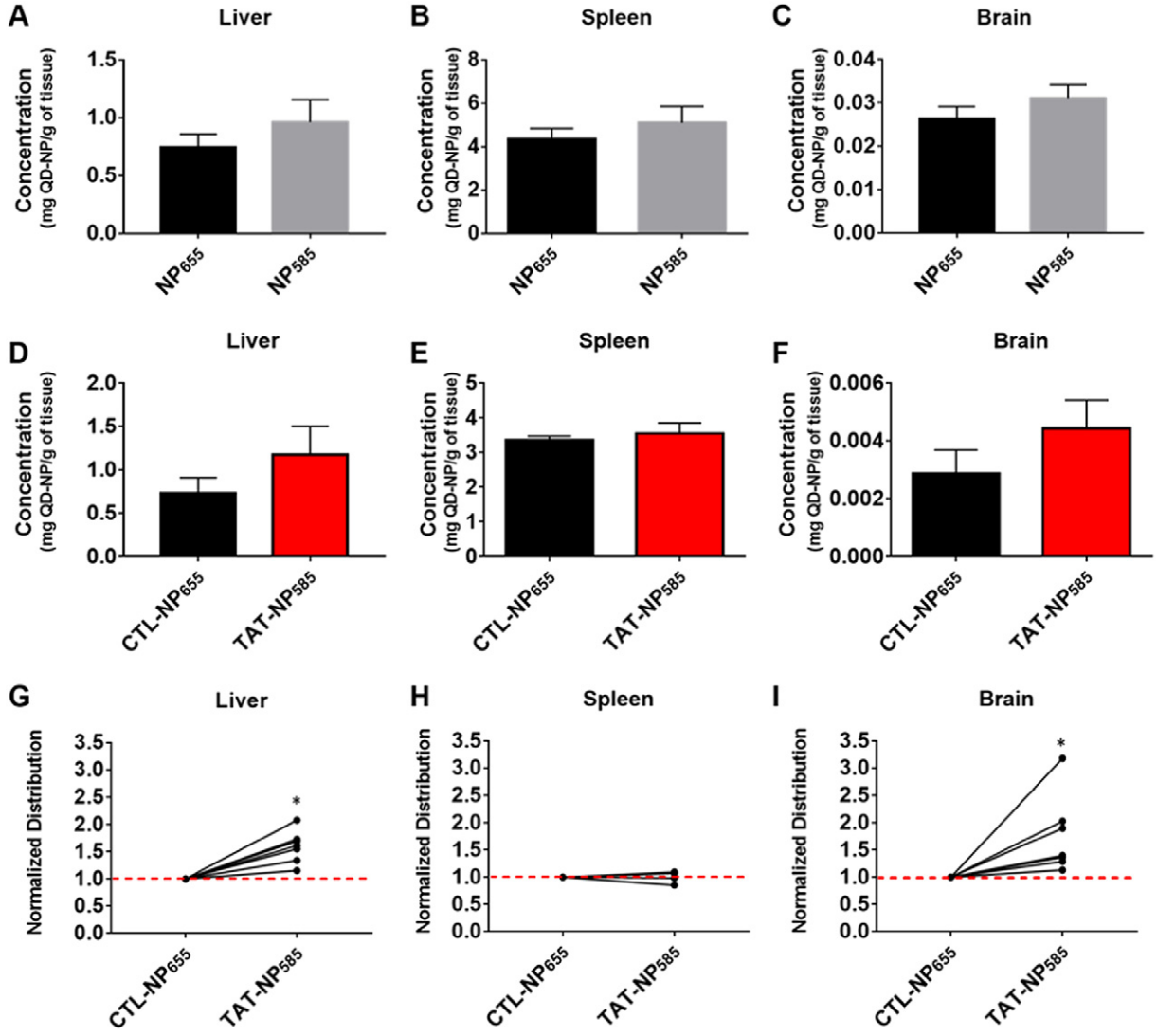

Fig. 4. Quantitative biodistribution measuring QD-NPs extracted from peripheral and CNS tissue. (A–C) Non-modified QD-NPs are equivalently distributed in the liver, spleen and brain n = 7 ($p > 0.05$, two-tailed *t*-test, for both paired and unpaired analyses), demonstrating the type of QD used to label nanoparticles does not significantly alter tissue level distribution. (D–F) QD-labeling can be used to measure levels of control nanoparticles ($CTL\text{-}NP_{655}$) *vs* targeted ($TAT\text{-}NP_{585}$). When data were analyzed by two-tailed *t*-test on unpaired/group sample means, no significant differences were detected between targeted and non-targeted formulations ($p > 0.05$). (G–I) Within-subject normalized distribution of $TAT\text{-}NP_{585}$:$CTL\text{-}NP_{655}$; lines connecting points represent the fold differences in concentrations of different QD-NPs within the same subject. Normalization reveals increased delivery of the targeted formulation ($TAT\text{-}NP_{585}$) compared to control ($CTL\text{-}NP_{655}$) within individual subjects; these differences were significant in liver and brain ($p = 0.027$ and $p = 0.017$, respectively, two-tailed *t*-test on paired samples). Error bars represent standard error of the mean in A–F.

or type of QD label significantly alters tissue accumulation of nanoparticles. These data thus open the possibility that differently labeled QD-nanoparticles can be utilized to quantify nanoparticle distribution of different polymer nanoparticle formulations in the same subject. To that end, we administered 2 different formulations of QD-NPs: one nanoparticle was labeled with QD_{585} and surface-modified with the trans-activator of transcription (TAT), a cell penetrating peptide ($TAT\text{-}NP_{585}$), and another nanoparticle was labeled with QD_{655} and surface-modified with biotin as a control ($CTL\text{-}NP_{655}$). These formulations were mixed together prior to injection to perform a biodistribution analysis. Of note, although liver and spleen accumulation of $CTL\text{-}NP_{655}$ were similar in magnitude to previous measurements conducted on NP_{585} and NP_{655}, the brain concentration of $CTL\text{-}NP_{655}$ – which are surface modified with avidin – was substantially lower than what was measured in the prior experiments (Fig. 4D–F). This reduction in delivery could either be due to more rapid clearance of the avidin modified nanoparticles from systemic circulation or due underlying differences in the ability of nanoparticles to interact with brain vasculature, specifically. In either case, our data suggest that avidin modification effectively reduces the already-low concentration of nanoparticles measured in whole brain homogenate. With respect to targeting, we found increases in the average concentrations of $TAT\text{-}NP_{585}$ in the liver, 1.18 ± 0.18 mg/g compared to $CTL\text{-}NP_{655}$, 0.73 ± 0.32 mg/g. We also found increases of $TAT\text{-}NP_{585}$ in the brain, 0.0044 ± 0.001 mg/g, compared to $CTL\text{-}NP_{655}$, 0.0029 ± 0.001 mg/g (Fig. 4F). These differences were not statistically significant when analyzed as a group average ($p = 0.25$ and 0.60 for liver and brain, respectively, unpaired 2-tailed Student's *t*-test). However, once the paired nature of the data was taken into consideration, targeting effects were found to be significant at a robust statistical level ($p = 0.027$ and 0.017 for liver and brain, respectively, paired 2-tailed Student's *t*-test); the robustness of targeting within individual subjects is visually evident when the data are normalized to their within-subject control (Fig. 4G–I). There was no relationship between magnitude of delivery and magnitude of targeting for individual subjects. This multispectral approach both permits direct comparison of control and targeted formulations over subcellular scales, and it also enables us to engage in quantitative measurement of multiple nanoparticles within a single subject. We are thus able to control for subject-to-subject variability due to measurement (*e.g.*, injection, perfusion) or biology (*e.g.*, differences in circulation time, immune response, or disease progression).

Previous work from our lab supports a model in which nanoparticles do not require internalization to deliver encapsulated payloads, where targeting is achieved by increasing the interaction of nanoparticles with cell surfaces to facilitate payload transfer [11]; however, the data supporting this model were relatively indirect, relying on analysis of the different kinetics of different payloads loaded into the nanoparticles. The new data shown here provide direct evidence that it will take several hours for a nanoparticle to be internalized (*i.e.*, Fig. 2B). We were thus interested to use the multispectral approaches to probe for differences in nanoparticle association with cells as a function of targeting under flow conditions that would better mimic the *in vivo* context. We first seeded murine brain endothelial cells (bEnd.3s) onto the surface of a laminar flow chamber; next, $TAT\text{-}NP_{655}$ and $CTL\text{-}NP_{585}$ were resuspended in 1% FBS and flushed across the surface of the cells a rate of either 0.25, 1, or 4 mL/min. These flow rates were chosen because they produce a range of sheer stress (1–15 dyn/cm^2) observed in cerebral blood vessels [29]. Live cell imaging demonstrated that, for every flow rate and over a course of 15 min, both formulations associated with the surface of bEnd.3 cells. However, a substantially higher quantity of $TAT\text{-}NP_{655}$ attached compared to $CTL\text{-}NP_{585}$; these differences are visually quite significant in the live imaging video (Fig. 5, Fig. S6–7, and Supplementary Video 1). Interestingly, while higher flow rates produced a mild increase in surface presence of $CTL\text{-}NP_{585}$, increasing flow produced a larger increase in $TAT\text{-}NP_{655}$ (Fig. S7). These data suggest that TAT-NPs possess a more frequent biophysical association with cell surfaces than CTL-NPs, even over time periods far shorter than required for nanoparticle internalization. Most significantly, the surface association of TAT-NPs may also be more robust under conditions of high, laminar flow. Collectively, these experiments provide early insight into the mechanisms by which targeted nanoparticles might enhance payload delivered across cells under convective flow, even in absence of transcytosis, and further emphasize the usefulness of utilizing within-sample controls.

3.4. Imaging to assess nanoparticle entry into the central nervous system

It has been demonstrated that encapsulation of active molecules within solid polymer nanoparticles can improve function of drugs to enable better therapy of diseases affecting the brain [1,3]. However, intense debate remains regarding whether such improvements reflect movement of the nanoparticles themselves across the BBB *versus* some non-specific phenomenon, such as enhanced availability/activity of molecules at the BBB. Our data suggest that movement of PLGA nanoparticles across an intact BBB is minimal. Nanoparticles are not reliably identifiable in the brain, and those that we can find remain directly associated with CD31+ vasculature (Fig. 6). However, closer analysis demonstrates very consistent nanoparticle delivery to circumventricular organs, such as the choroid plexus (Fig. 6). These data confirm prior reports suggesting increased access of nanoparticulate systems to the brain *via* the choroid plexus [30] and suggest that cerebrospinal fluid (CSF) could facilitate delivery of a small number of nanoparticles to CSF exposed tissue.

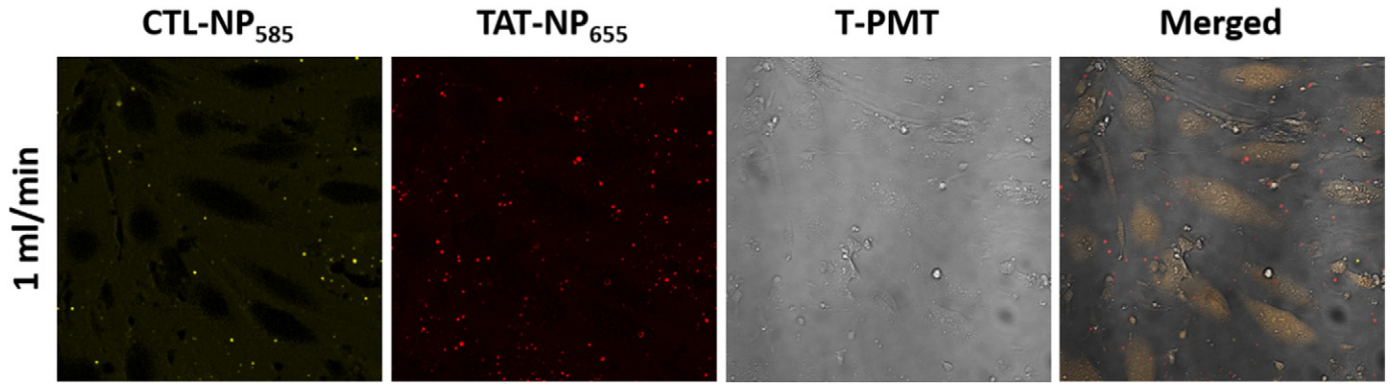

Fig. 5. Targeted nanoparticles have increased interactions with bEnd.3 cells in laminar flow conditions. Images demonstrate that that $TAT\text{-}NP_{655}$ (red) bind to cells at much higher rates than $CTL\text{-}NP_{585}$ (yellow). Images were acquired by averaging the last 50 frames of 900 taken over 15 min under a flow rate of 1.0 mL/min. Scale bar = 20 μm.

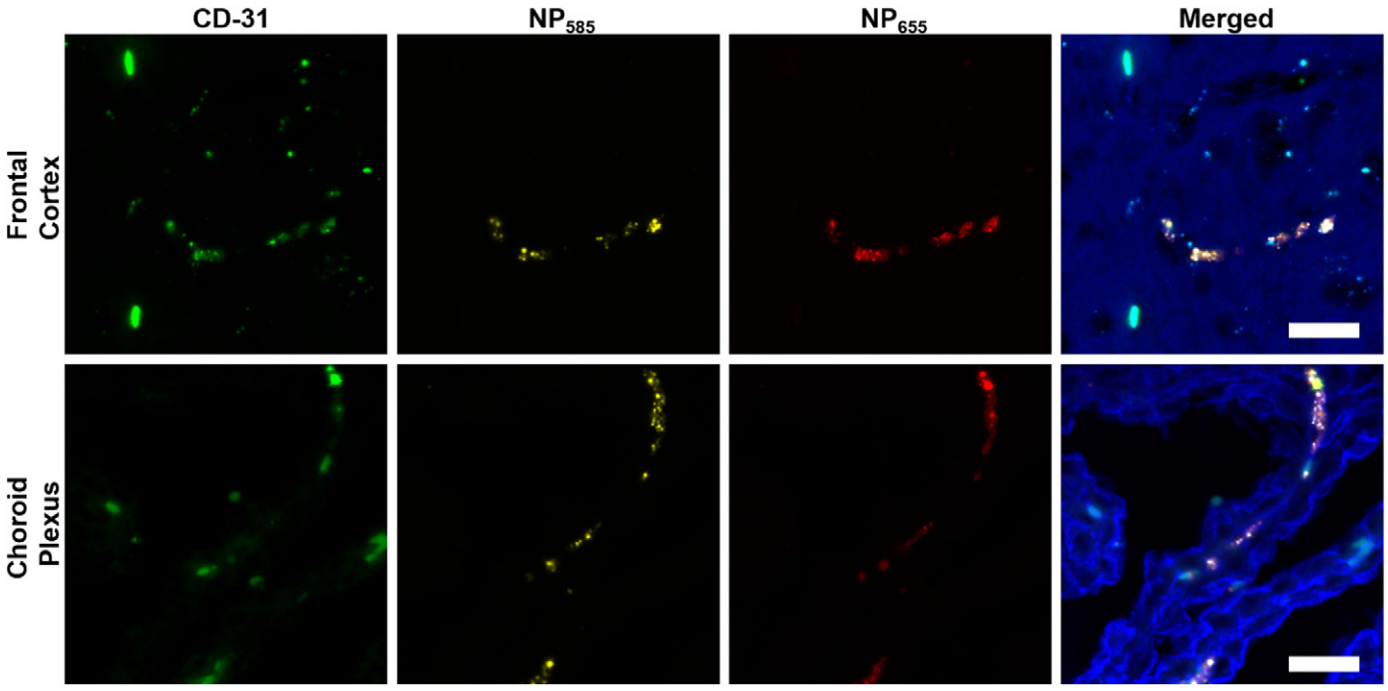

Fig. 6. Tracking of QD-NP delivery in the CNS. NP_{585} (yellow) and NP_{655} (red) do not readily cross into the parenchyma of healthy CNS tissue. Confocal microscopy reveals sporadic distribution throughout the brain is associated with blood vessel marker CD-31 (green); Phalloidin (blue). Scale bar = 25 μm.

Our motivation for developing better methods to localize nanoparticles *in vivo* is the expectation that this will enable evaluation of their delivery to or across the BBB independently from the pharmacokinetic behavior of individual drug payloads [11,13]. This approach could dramatically improve our ability to test and develop generalizable methods for delivering drugs to the CNS. When TAT-modified nanoparticles were administered to healthy mice, we observed no evidence for their entry into the parenchyma; delivery was, as before, confined to CD31+ vasculature and circumventricular organs. To determine whether nanoparticle localization would be altered by disease-induced disruption of the BBB, QD-NPs were administered to mice bearing late-stage, intracranial GL261 tumors. The GL261 (mouse glioma cell line) tumor model was used as a disease model because it exhibits increased vascularity within the tumor mass, which mimics human glioblastoma multiforme tumors [3]. In these subjects, nanoparticles were observed throughout the tumor core 2 h after injection (Fig. 7). Nanoparticles were never observed beyond CD31+ vasculature, even at later time points (*e.g.*, up to 24 h later, data not shown).

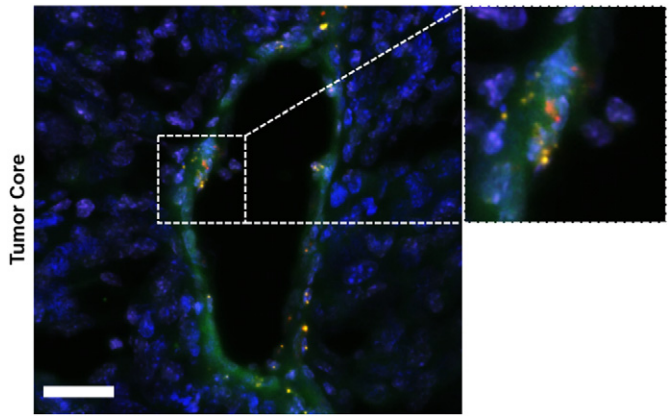

Fig. 7. Administration of NP_{585} (yellow) and NP_{655} (red) into intracranial tumor bearing mice revealed widespread distribution of QD-NPs especially throughout the tumor core; DAPI (blue). Box area reveals QD-NPs associated with CD-31 (green). Scale bar = 20 μm.

Thus, increased vascularity within the tumor core does not necessarily enable unhindered access of nanoparticles to the parenchyma but instead facilitates nanoparticle entrapment within or between endothelial cells in this tumor model. Increased association of nanoparticles with brain endothelial cells would provide a higher source concentration of payload in close proximity to tumor tissue; this model is thus consistent with increased delivery of nanoparticle encapsulated payloads that we and others have observed in highly vascularized tumors [3,31]. Ultimately, the entry of systemically administered, solid nanoparticles into the brain parenchyma is minimal, which supports a model for brain delivery that is in fact achieved *via* nanoparticle association with the surface of brain vasculature and opens the possibility for delivery to circumventricular organs [11].

These studies provide direct evidence that the use of fluorescent dyes to track nanoparticle distribution *in vitro* and *in vivo* can give misleading information in regards to localization of individual nanoparticles. Prior studies using nanoparticles, including PLGA nanoparticles, demonstrate that rapid delivery of hydrophobic dyes and payloads are primarily due to contact based transfer of dye from nanoparticles to cell membranes [11,13]. This makes interpretation of studies using these encapsulated dyes more complicated than just internalization of nanoparticles. For example, studies that demonstrate targeting by modification of nanoparticles should acknowledge that any increases in payload delivery may be reflective of increased interaction of nanoparticles with cells or tissue or altered release of the payload, rather than the internalization or transport of the nanoparticle itself across a biological barrier.

Taken in sum, we developed a labeling strategy that enables quantitative nanoparticle tracking with much higher spatial resolution and sensitivity than traditional methods. We also demonstrate that multiple nanoparticle formulations can be barcoded with distinct color labels and tracked simultaneously within individual samples *in vitro* and *in vivo*. Recently, Dahlman, et al. developed a strategy to compare multiple lipid nanoparticles in single samples through encapsulation of nucleic acid barcodes; they demonstrated comparison of 30 formulations from

whole tissue homogenates in a single mouse, which highlights the potential for alternative approaches to enable higher throughput evaluation of nanoparticle delivery [33]. One advantage of our covalent strategy is that the QD labeling permits spatial analyses of nanoparticle interaction with tissue- and cellular-level barriers. QDs have been used by others for labeling and tracking of different macromolecules *in vivo* and *in vitro* [14,28,34], and previous reports have demonstrated the ability to track nanoparticles using conjugated and encapsulated QDs *in vitro* [25,35]. However, although *in vivo* tracking of free QD has been demonstrated with high resolution [36], to our knowledge, QD covalently-labeled polymeric nanoparticles have not been previously reported *in vivo*. Future work may yield opportunities to engineer nanoparticles to overcome the limitations observed here; for example, the large size (~250 nm) of our formulation may prevent effective movement into brain parenchyma [32], or alternative targeting approaches might reveal new opportunities to facilitate nanoparticle movement across biological barriers [37].

4. Conclusions

To better engineer nanoparticles for delivery across biological barriers, it is critical to understand the fate of nanoparticles in cells and tissue [11,13,16]. Our experiments demonstrate a novel, multispectral approach for tracking multiple nanoparticle formulations *in vitro* and *in vivo* with high spatial resolution and detection sensitivity. We show that the wavelength of QD used to labeled nanoparticles does not affect nanoparticle physiochemical properties, cellular uptake, or *in vivo* distribution. QD-NPs of multiple wavelengths were used to assess qualitative and quantitative measures of delivery for multiple formulations within a single subject. We also show that using within-subject controls improves our ability to detect targeting effects *in vivo*. QD-labeling of nanoparticles thus offers an excellent tool to answer questions of regarding the interaction of nanoparticles with cells and tissues.

Supplementary data to this article can be found online at http://dx.doi.org/10.1016/j.jconrel.2017.02.033.

Author contributions

The manuscript was written by David X. Medina and Rachael W. Sirianni. Research was primarily carried out and managed by David X. Medina. Kyle T. Householder provided technical support and performed tumor inductions. Ricki Ceton performed immunofluorescence and biodistribution studies. Tina Kovalik performed cell viability assays. John Heffernan provided technical support of conjugation chemistry and performed NMR. Rohini V. Shankar provided TEM imaging. Robert P. Bowser and Robert J. Wechsler-Reya provided vital intellectual contributions in the development of the project. Rachael Sirianni was primary investigator on project. All authors have given approval to the final version of the manuscript.

Abbreviations

QD	quantum dots
NP	nanoparticles
QD-NP	quantum dot-labeled nanoparticles
PLGA	poly(lactic-co-glycolic) acid

Acknowledgment

We gratefully acknowledge the funding from the Barrow Neurological Foundation, the U.S. Department of Defense (W81XWH-14-0311), the Amyotrophic Lateral Sclerosis Association (ALSA) Milton Safenowitz Postdoctoral Fellowship (Grant ID: 8417) and the Arizona State University. We thank V. Kodibagkar at Arizona State University for assistance with the transmission electron microscopy experiments.

References

[1] J. Kreuter, Drug delivery to the central nervous system by polymeric nanoparticles: what do we know? Adv. Drug Deliv. Rev. 71 (2014) 2–14, http://dx.doi.org/10.1016/j.addr.2013.08.008.
[2] T. Patel, J. Zhou, J.M. Piepmeier, W.M. Saltzman, Polymeric nanoparticles for drug delivery to the central nervous system, Adv. Drug Deliv. Rev. 64 (2012) 701–705, http://dx.doi.org/10.1016/j.addr.2011.12.006.
[3] K.T. Householder, D.M. DiPerna, E.P. Chung, G.M. Wohlleb, H.D. Dhruv, M.E. Berens, R.W. Sirianni, Intravenous delivery of camptothecin-loaded PLGA nanoparticles for the treatment of intracranial glioma, Int. J. Pharm. 479 (2015) 374–380, http://dx.doi.org/10.1016/j.ijpharm.2015.01.002.
[4] A. Kumari, S.K. Yadav, S.C. Yadav, Biodegradable polymeric nanoparticles based drug delivery systems, Colloids Surf. B: Biointerfaces 75 (2010) 1–18, http://dx.doi.org/10.1016/j.colsurfb.2009.09.001.
[5] I. Bala, S. Hariharan, M.N.V.R. Kumar, PLGA nanoparticles in drug delivery: the state of the art, Crit. Rev. Ther. Drug Carrier Syst. 21 (2004) 387–422.
[6] N. Bertrand, J. Wu, X. Xu, N. Kamaly, O.C. Farokhzad, Cancer nanotechnology: the impact of passive and active targeting in the era of modern cancer biology, Adv. Drug Deliv. Rev. 66 (2014) 2–25, http://dx.doi.org/10.1016/j.addr.2013.11.009.
[7] Y. Chen, L. Liu, Modern methods for delivery of drugs across the blood–brain barrier, Adv. Drug Deliv. Rev. 64 (2012) 640–665, http://dx.doi.org/10.1016/j.addr.2011.11.010.
[8] J. Panyam, V. Labhasetwar, Biodegradable nanoparticles for drug and gene delivery to cells and tissue, Adv. Drug Deliv. Rev. 55 (2003) 329–347, http://dx.doi.org/10.1016/S0169-409X(02)00228-4.
[9] M. Li, H. Deng, H. Peng, Q. Wang, Functional nanoparticles in targeting glioma diagnosis and therapies, J. Nanosci. Nanotechnol. 14 (2014) 415–432, http://dx.doi.org/10.1166/jnn.2014.8757.
[10] M.M.A. Abdel-Mottaleb, A. Beduneau, Y. Pellequer, A. Lamprecht, Stability of fluorescent labels in PLGA polymeric nanoparticles: quantum dots versus organic dyes, Int. J. Pharm. 494 (2015) 471–478, http://dx.doi.org/10.1016/j.ijpharm.2015.08.050.
[11] R.L. Cook, K.T. Householder, E.P. Chung, A.V. Prakapenka, D.M. DiPerna, R.W. Sirianni, A critical evaluation of drug delivery from ligand modified nanoparticles: confounding small molecule distribution and efficacy in the central nervous system, J. Control. Release 220 (2015) 89–97, http://dx.doi.org/10.1016/j.jconrel.2015.10.013.
[12] P. Pietzonka, B. Rothen-Rutishauser, P. Langguth, H. Wunderli-Allenspach, E. Walter, H.P. Merkle, Transfer of lipophilic markers from PLGA and polystyrene nanoparticles to Caco-2 monolayers mimics particle uptake, Pharm. Res. 19 (2002) 595–601, http://dx.doi.org/10.1023/A:1015393710253.
[13] P. Xu, E. Gullotti, L. Tong, C.B. Highley, D.R. Errabelli, T. Hasan, J.-X. Cheng, D.S. Kohane, Y. Yeo, Intracellular drug delivery by poly(lactic- co -glycolic acid) nanoparticles, revisited, Mol. Pharm. 6 (2009) 190–201, http://dx.doi.org/10.1021/mp800137z.
[14] U. Resch-Genger, M. Grabolle, S. Cavaliere-Jaricot, R. Nitschke, T. Nann, Quantum dots versus organic dyes as fluorescent labels, Nat. Methods 5 (2008) 763–775, http://dx.doi.org/10.1038/nmeth.1248.
[15] S. Wohlfart, S. Gelperina, J. Kreuter, Transport of drugs across the blood–brain barrier by nanoparticles, J. Control. Release 161 (2012) 264–273, http://dx.doi.org/10.1016/j.jconrel.2011.08.017.
[16] S. Florinas, M. Liu, R. Fleming, L. Van Vlerken-Ysla, J. Ayriss, R. Gilbreth, N. Dimasi, C. Gao, H. Wu, Z.-Q. Xu, S. Chen, A. Dirisala, K. Kataoka, H. Cabral, R.J. Christie, A nanoparticle platform to evaluate bioconjugation and receptor-mediated cell uptake using cross-linked polyion complex micelles bearing antibody fragments, Biomacromolecules 17 (2016) 1818–1833, http://dx.doi.org/10.1021/acs.biomac.6b00239.
[17] T.J. Deerinck, The application of fluorescent quantum dots to confocal, multiphoton, and electron microscopic imaging, Toxicol. Pathol. 36 (2008) 112–116, http://dx.doi.org/10.1177/0192623307310950.
[18] P. Pierobon, G. Cappello, Quantum dots to tail single bio-molecules inside living cells, Adv. Drug Deliv. Rev. 64 (2012) 167–178, http://dx.doi.org/10.1016/j.addr.2011.06.004.
[19] W.R. Algar, A.J. Tavares, U.J. Krull, Beyond labels: a review of the application of quantum dots as integrated components of assays, bioprobes, and biosensors utilizing optical transduction, Anal. Chim. Acta 673 (2010) 1–25, http://dx.doi.org/10.1016/j.aca.2010.05.026.
[20] L.D. True, X. Gao, Quantum dots for molecular pathology, J. Mol. Diagn. 9 (2007) 7–11, http://dx.doi.org/10.2353/jmoldx.2007.060186.
[21] S.O. Meade, M.Y. Chen, M.J. Sailor, G.M. Miskelly, Multiplexed DNA detection using spectrally encoded porous SiO2 photonic crystal particles, Anal. Chem. 81 (2009) 2618–2625, http://dx.doi.org/10.1021/ac802538x.
[22] R.L. McCall, R.W. Sirianni, PLGA nanoparticles formed by single- or double-emulsion with vitamin E-TPGS, J. Vis. Exp. (2013)http://dx.doi.org/10.3791/51015.
[23] J. Park, T. Mattessich, S.M. Jay, A. Agawu, W.M. Saltzman, T.M. Fahmy, Enhancement of surface ligand display on PLGA nanoparticles with amphiphilic ligand conjugates, J. Control. Release 156 (2011) 109–115, http://dx.doi.org/10.1016/j.jconrel.2011.06.025.
[24] M.G. Abdelwahab, T. Sankar, M.C. Preul, A.C. Scheck, Intracranial implantation with subsequent 3D in vivo bioluminescent imaging of murine gliomas, J. Vis. Exp. (2011), e3403. http://dx.doi.org/10.3791/3403.
[25] S. Marrache, S. Dhar, Engineering of blended nanoparticle platform for delivery of mitochondria-acting therapeutics, Proc. Natl. Acad. Sci. 109 (2012) 16288–16293, http://dx.doi.org/10.1073/pnas.1210096109.
[26] A. Valizadeh, H. Mikaeili, M. Samiei, S. Farkhani, N. Zarghami, M. Kouhi, A. Akbarzadeh, S. Davaran, Quantum dots: synthesis, bioapplications, and toxicity, Nanoscale Res. Lett. 7 (2012) 480, http://dx.doi.org/10.1186/1556-276X-7-480.
[27] F. Pederzoli, B. Ruozi, E. Pracucci, G. Signore, M. Zapparoli, F. Forni, M.A. Vandelli, G. Ratto, G. Tosi, Nanoimaging: photophysical and pharmaceutical characterization of

poly-lactide-co-glycolide nanoparticles engineered with quantum dots, Nanotechnology 27 (2016) 015704, http://dx.doi.org/10.1088/0957-4484/27/1/015704.
[28] K.M. Tsoi, Q. Dai, B.A. Alman, W.C.W. Chan, Are quantum dots toxic? Exploring the discrepancy between cell culture and animal studies, Acc. Chem. Res. 46 (2013) 662–671, http://dx.doi.org/10.1021/ar300040z.
[29] A. Wong, M. Ye, A. Levy, J. Rothstein, D. Bergles, P.C. Searson, The blood-brain barrier: an engineering perspective, Front. Neuroengineering 6 (2013), http://dx.doi.org/10.3389/fneng.2013.00007.
[30] Z.H. Wang, Z.Y. Wang, C.S. Sun, C.Y. Wang, T.Y. Jiang, S.L. Wang, Trimethylated chitosan-conjugated PLGA nanoparticles for the delivery of drugs to the brain, Biomaterials 31 (2010) 908–915, http://dx.doi.org/10.1016/j.biomaterials.2009.09.104.
[31] E.J. Chung, Y. Cheng, R. Morshed, K. Nord, Y. Han, M.L. Wegscheid, B. Auffinger, D.A. Wainwright, M.S. Lesniak, M.V. Tirrell, Fibrin-binding, peptide amphiphile micelles for targeting glioblastoma, Biomaterials 35 (2014) 1249–1256, http://dx.doi.org/10.1016/j.biomaterials.2013.10.064.
[32] M. Shilo, A. Sharon, K. Baranes, M. Motiei, J.-P.M. Lellouche, R. Popovtzer, The effect of nanoparticle size on the probability to cross the blood-brain barrier: an in-vitro endothelial cell model, J. Nanobiotechnology 13 (2015) 19, http://dx.doi.org/10.1186/s12951-015-0075-7.
[33] J.E. Dahlman, K.J. Kauffman, Y. Xing, T.E. Shaw, F.F. Mir, C.C. Dlott, R. Langer, D.G. Anderson, E.T. Wang, Barcoded nanoparticles for high throughput in vivo discovery of targeted therapeutics, Proc. Natl. Acad. Sci. 114 (2017) 2060–2065, http://dx.doi.org/10.1073/pnas.1620874114.
[34] J.B. Delehanty, K. Susumu, R.L. Manthe, W.R. Algar, I.L. Medintz, Active cellular sensing with quantum dots: transitioning from research tool to reality; a review, Anal. Chim. Acta 750 (2012) 63–81, http://dx.doi.org/10.1016/j.aca.2012.05.032.
[35] F.-Y. Cheng, S.P.-H. Wang, C.-H. Su, T.-L. Tsai, P.-C. Wu, D.-B. Shieh, J.-H. Chen, P.C.-H. Hsieh, C.-S. Yeh, Stabilizer-free poly(lactide-co-glycolide) nanoparticles for multimodal biomedical probes, Biomaterials 29 (2008) 2104–2112, http://dx.doi.org/10.1016/j.biomaterials.2008.01.010.
[36] S. Sindhwani, A.M. Syed, S. Wilhelm, D.R. Glancy, Y.Y. Chen, M. Dobosz, W.C.W. Chan, Three-dimensional optical mapping of nanoparticle distribution in intact tissues, ACS Nano 10 (2016) 5468–5478, http://dx.doi.org/10.1021/acsnano.6b01879.
[37] R.L. McCall, J. Cacaccio, E. Wrabel, M.E. Schwartz, T.P. Coleman, R.W. Sirianni, Pathogen-inspired drug delivery to the central nervous system, Tissue Barriers 2 (2014), e944449. http://dx.doi.org/10.4161/21688362.2014.944449.